

Effect of Spontaneously Generated Coherence and detuning on 2D Atom Localization in Two Orthogonal Standing-wave Fields*

Shun-Cai Zhao^{1,†}, Qi-Xuan Wu,² and Ai-Ling Gong¹

¹*Department of Physics, Faculty of Science, Kunming University of Science and Technology, Kunming, 650500, PR China*

²*College English department, Kunming University of Science and Technology, Kunming, 650500*

Two-dimensional(2D)atom localization via the spontaneously generated coherence (SGC) and detunings associated with the probe and standing-wave driving fields in a three-level V-type atomic system is investigated. In the gain process, two equal and tunable peak maximums of position distribution in the x-y plane via the detunings are observed. However, one decreasing and other increasing peak maximums in the absorption process via the spontaneously generated coherence(SGC) are achieved in the quadrants I and III of the x-y plane. A better resolution and more novelty for 2D atom localization in our scheme is obtained.

Subwavelength atom localization has become an active research topic from both the theoretical and experimental points of view, because of its applications in the laser cooling and trapping of neutral atoms^[1,2], atom lithography^[3], measurement of atomic wave function^[4], etc.. Several schemes utilized a standing-wave field^{[5]–[14]} for atom localization have been proposed since the position-dependent atom-field interaction, such as the effect of spontaneous emission^[6,7], population^[8,10,12,14], absorption^[9], the entanglement between the atom's internal states and its position^[15], phase shift of the field^[16] and gain^[17] on the atomic position information was discussed. Recently, one-dimensional (1D) sub-half-wavelength atom localization was achieved^[17–25] by interacting with two standing-wave fields. The resulting quantities, for instance, the homodyne detection^[5], Raman gain process^[7], phase shift^[1,18], probe field absorption^[9,20], quantum trajectories^[21], upper level population^[8,21], dual quadrature field^[22], two-photon spontaneous emission^[23], coherent population trapping^[24] and the superposition of two standing-wave fields^[25] can provide the one-dimensional(1D) atomic position information. In the same way, the 2D atom localization was achieved utilizing multiple simultaneous quadrature measurement, the

population in the upper state or in any ground state measurement, probe absorption measurement and incorporating the quantum interference phenomenon measurement, respectively^[26–29]. And other schemes^[30–34] for 2D atom localization were also proposed in recent years. Such as in the coherently driven cycle-configuration and a five-level M-type atomic systems are proposed for 2D atom localization based on controllable spontaneous emission^[30,32].

However, spontaneously generated coherence (SGC) refers to the interference of spontaneous emission channels^[35] firstly showed by Agarwal^[36] in a degenerate Λ -type three-level atom system, and which plays an important role^[37–45] in lasing without population inversion, coherent population trapping(CPT), group velocity reduction, ultra fast all-optical switching and transparent high-index materials, high-precision spectroscopy and magnetometer and modified quantum beats, etc. Inspired by these investigations, we here utilize the two interference of spontaneous emission channels to explore an interesting scheme for 2D atom localization. When the two orthogonal standing-wave fields drive the same atomic transition in the Λ -type atom, two equal and tunable peaks of the position probability distribution occur in quadrants I and III when manipulating

the detunings corresponding to the probe and the coupled orthogonal standing-wave fields. However, when the SGC intensities were varied, one decreasing and other increasing peak maximums of 2D atom localization in the quadrants I and III of x-y plane appear. Comparing our atomic scheme and the traditional 2D atom localization schemes [26–28], the results show noticeably an increasing spatial resolution and high precision, and manifest much more flexibility and novelty.

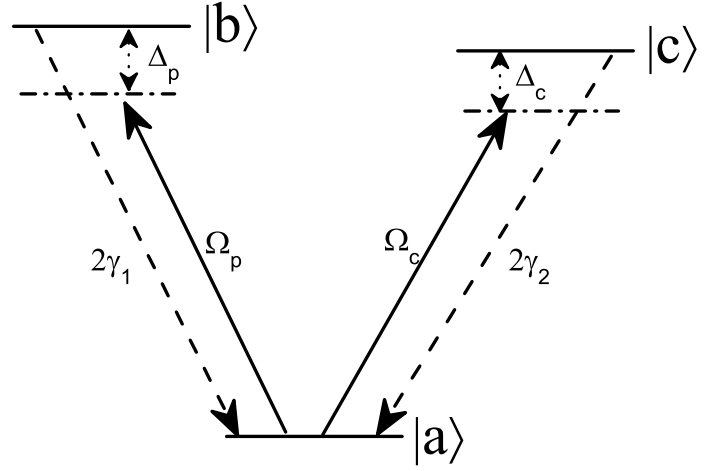


Fig. 1. Level diagram of the atomic system: Two orthogonal standing waves fields having position-dependent Rabi $\Omega_c(x, y)$ corresponding to the atomic transition from $|c\rangle$ to $|a\rangle$. A weak probe field Ω_p couples the transition from $|a\rangle$ to $|b\rangle$. $2\gamma_1$ and $2\gamma_2$ are the atomic decay rates.

We consider a V-type system[see Fig.1] which has a lower state $|a\rangle$ and two excited states $|c\rangle$ and $|b\rangle$. A weak probe field with frequency ν_p and Rabi frequency E_p of $\Omega_p = E_p\mu_{ab}/2\hbar$ drives the transition $|a\rangle \leftrightarrow |b\rangle$ with frequency ω_{ab} . And a strong coherent coupling standing-wave field $E_{x,y}$ with the same frequency ν_c is simultaneously applied to the transition $|a\rangle \leftrightarrow |c\rangle$ with frequency ω_{ac} . The Rabi frequency $\Omega_c(x, y)$ corresponding to the composition of two orthogonal standing waves is $\Omega_c(x, y) = E_{x,y}\mu_{ac}/2\hbar = \Omega_0[\sin(\kappa_1x + \delta) + \sin(\kappa_2y + \eta)]$. Where μ_{ab} and μ_{ac} are the corresponding dipole matrix elements, $\kappa_i = 2\pi/\lambda_i$, ($i = 1, 2$) is the wave vector with wavelengths λ_i , ($i = 1, 2$) of the corresponding standing wave fields. For simplicity, we assume Ω_p and Ω_0 to be real. $\Delta_p = \omega_{ab} - \nu_p$, and $\Delta_c = \omega_{ac} - \nu_c$ are the detunings of the two corresponding fields, respectively. $2\gamma_1$ and $2\gamma_2$ are the spontaneous decay rates of the excited state $|c\rangle$ and $|b\rangle$ to the ground states $|a\rangle$, respectively. When the two excited levels $|c\rangle$ and $|b\rangle$ are closely spaced such that the two transitions to the lower state interact with the same vacuum mode, SGC can be present.

Even though there is a principle difficulty in the realization of atomic interference via spontaneous emission for atomic transitions in free space, the technique of photonic band-gap materials and semiconductor quantum dots was proposed to realize the interference[46]. Since the pseudophotonic band-gap structures have a special purpose[47], which can allow the propagation of electromagnetic waves with a certain polarization and strongly forbid those with orthogonal polarizations. So, the spontaneous decay with forbidden polarization is also forbidden and this allows us to remove the cancellation of different contributions originated from different polarizations of spontaneous emission occurring in free space, which is just what we need.

Along the directions of the standing waves, the center-of-mass position of the atomic is assumed to be nearly constant. Hence, the Raman-Nath approximation is applied and the kinetic energy of the atom in the Hamiltonian is ignored[27,48]. Under the electric dipole and rotating-wave approximation, we write the systematic density matrix in

the interaction picture involving the SGC as^[49–50]

$$\dot{\rho}_{cc} = -2\gamma_1\rho_{cc} + i\Omega_c(\rho_{ac} - \rho_{ca}) - p\sqrt{\gamma_1\gamma_2}(\rho_{cb} + \rho_{bc}) \quad (1)$$

$$\dot{\rho}_{bb} = -2\gamma_1\rho_{bb} + i\Omega_p(\rho_{ab} - \rho_{ba}) - p\sqrt{\gamma_1\gamma_2}(\rho_{cb} + \rho_{bc}) \quad (2)$$

$$\begin{aligned} \dot{\rho}_{ac} = & -(\gamma_1 + i\Delta_c)\rho_{ac} - p\sqrt{\gamma_1\gamma_2}\rho_{ab} + i\Omega_c(\rho_{cc} - \rho_{aa}) \\ & + i\Omega_p\rho_{bc}, \end{aligned} \quad (3)$$

$$\begin{aligned} \dot{\rho}_{cb} = & i\Omega_c\rho_{ab} - i\Omega_p\rho_{ca} - i(\Delta_p - \Delta_c)\rho_{cb} - (\gamma_1 + \gamma_2)\rho_{cb} \\ & - p\sqrt{\gamma_1\gamma_2}(\rho_{cc} + \rho_{bb}), \end{aligned} \quad (4)$$

$$\begin{aligned} \dot{\rho}_{ab} = & -p\sqrt{\gamma_1\gamma_2}\rho_{ac} - (\gamma_2 + i\Delta_p)\rho_{ab} + i\Omega_c\rho_{cb} \\ & + i\Omega_p(\rho_{bb} - \rho_{aa}). \end{aligned} \quad (5)$$

along with the the requirement of closing system, i.e., $\rho_{aa} + \rho_{bb} + \rho_{cc} = 1$ and $\rho_{ij}^* = \rho_{ji}$. And in which the parameter p denoting the alignment of the two dipole moments is defined as $p = \vec{\mu}_{ab} \cdot \vec{\mu}_{ac} / |\vec{\mu}_{ab} \cdot \vec{\mu}_{ac}| = \cos\theta$ with θ being the angle between the two dipole moments μ_{ac} and μ_{ab} , which can be a random angle between 0 and 2π except for 0 and π , and which is very sensitive for the existence of the SGC effect. The terms with $p\sqrt{\gamma_1\gamma_2}$ represent the quantum interference resulting from the cross coupling between spontaneous emission paths $|a\rangle$ - $|c\rangle$ and $|a\rangle$ - $|b\rangle$. It should be noted that only for small energy spacing between the two excited levels are the interference terms in the systematic density matrix significant; otherwise the oscillatory terms will average out to zero and thereby the SGC effect vanishes.

The information about the 2D atomic position from the susceptibility^[22] of the system at the probe field frequency is what we want to get. The nonlinear Raman susceptibility χ is then given by

$$\chi = \frac{2N|\mu_{ab}|^2}{\epsilon_0\Omega_P\hbar}\rho_{ab}, \quad (6)$$

where N is the atom number density in the medium and μ_{ab} is the magnitude of the dipole-matrix element between

$|a\rangle$ and $|b\rangle$. ϵ_0 is the permittivity in free space. The general steady-state analytical solution for ρ_{ab} can be written as

$$\rho_{ab}^1 = \frac{-4B_7 + \Omega_p\{-B_1\rho_{ac}^0 + \Omega_c[-i(B_0 - B_5)p\rho_{ba}^0]\}}{4[-p^2B_8 + B_{10}p^4 - 4p^6 + B_9(1 + \Delta_c^2 + 2\Omega_c^2)]} \quad (7)$$

with

$$\rho_{ac}^0 = \frac{(\Delta_p - i)(\Delta_p - 2i - \Delta_c)\Omega_c - \Omega_c^3}{(2i + \Delta_c - \Delta_p)[p^2 + (\Delta_p - i)(\Delta_c - i)] + (\Delta_c - i)\Omega_c^2}, \quad (8)$$

$$\rho_{ab}^0 = \frac{p\Omega_c(2i + \Delta_c - \Delta_p)}{(2i + \Delta_c - \Delta_p)[ip^2 - i + \Delta_c(1 + i\Delta_p) + \Delta_p] + (1 + i\Delta_c)\Omega_c^2}, \quad (9)$$

$$\rho_{cb}^0 = \frac{ip\Omega_c^2}{(2i + \Delta_c - \Delta_p)[p^2 + (\Delta_p - i)(\Delta_c - i)] + (\Delta_c - i)\Omega_c^2}, \quad (10)$$

$$\rho_{ab}^1 = -p\sqrt{\gamma_1\gamma_2}\rho_{ac} - (\gamma_2 + i\Delta_p)\rho_{ab} + i\Omega_c\rho_{cb} + i\Omega_p(\rho_{bb} - \rho_{aa}). \quad (11)$$

where the parameters B_i , ($i = 0, \dots, 10$) in Eq.(3) are given in the Appendix, and we have set $\gamma_1 = \gamma_2 = \gamma$. All the parameters are reduced to dimensionless units by scaling with γ . Using Eq.(2), which consists of both real and imaginary parts, i.e., $\chi = \chi' + i\chi''$. The imaginary part of the susceptibility gives the absorption profile of the probe field which can be written as

$$\chi'' = \frac{2N|\mu_{ab}|^2}{\epsilon_0\hbar} \text{Im}\left[\frac{\rho_{ab}}{\Omega_P}\right] = \alpha \text{Im}\left[\frac{\rho_{ab}}{\Omega_P}\right], \quad (12)$$

where $\alpha = \frac{2N|\mu_{ab}|^2}{\epsilon_0\hbar}$. Here we are interested in the 2D position measurement of the atom using the absorption process of the probe field. The Eq.(7) is the main result and reflects the conditional position probability distribution of the atom^[22]. It can be seen that the probe absorption depends on the position dependent the SGC intensities p and the detunings associated with the probe and standing-wave driving fields, therefore, we can obtain the 2D atomic position information by manipulating the corresponding parameters.

In this section, we analyze the imaginary part χ'' of the susceptibility depicting the absorption profile of the probe field which directly reflects the 2D atomic conditional position probability distribution, and then demonstrate a high resolution of 2D atom localization via manipulation of the

values of detunings or the the intensities p of SGC. It is evident that χ'' depends on the parameters of the field detunings and the intensities p of SGC, which can be seen from Eq.(3) to Eq.(6). However, the analytical expressions from Eq.(3) to Eq.(6) corresponding to the field detunings and the intensities p of SGC is rather cumbersome. Hence, the numerical approach was preferred to analyze the the 2D atomic position probability distribution via χ'' . In the following discussion, the probe field absorption χ'' reflecting different position probability distribution of the atom within optical wavelength domain is plotted.

Initially, the position dependent the probe field detuning Δ_p is considered. We set $\Delta_c=0$, and the Rabi frequency, $\Omega_{c0}=10\gamma$, $\Omega_{p0}=0.01\gamma$. Then a three-dimensional plot depicting the effect of position-dependent the probe detuning Δ_p for the imaginary susceptibility χ'' as a function of (x,y) is shown in Fig.2.

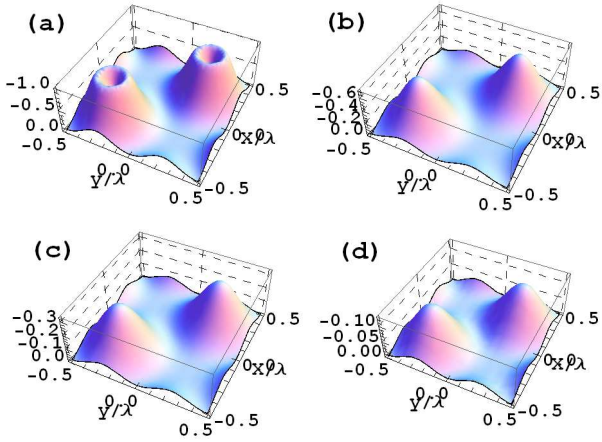


Fig. 2. (Color online) Plots for 2D atom localization: χ'' as a function of (x,y) in dependence on the probe detuning Δ_p . (a) $\Delta_p=21\gamma$,(b) $\Delta_p=30\gamma$, (c) $\Delta_p=40\gamma$, (d) $\Delta_p=60\gamma$. Parameters are $\kappa_1=\kappa_2=2\pi/\lambda$, $\Omega_{c0}=10\gamma$, $\Omega_{p0}=0.01\gamma$, $\Delta_c=0$, $\theta=0.5\pi$, and where γ is the scaling parameter.

As shown in Fig.2(a), a craterlike pattern occurs in the quadrants I and III and which leads to the localization of the atom at these circles with peak maxima being -1. An equal maximum probability is gotten in the

standing-wave plane. When $\Delta_p=30\gamma$ in Fig.2(b), the probability distribution changes into two spikelike patterns in the quadrants I and III of x - y plane. And the peak maxima declines sharply to -0.6. Increasing the probe detuning Δ_p repeatedly to $30\gamma, 40\gamma$ in Fig.2(c) and (d), the spike-like pattern remains but its peak maxima continues to decrease. And the corresponding maximum probabilities of 2D atom localization are -0.3, -0.1 in Fig. 2(c)and (d), respectively. So, when the probe field off-resonantly couples $|a\rangle\leftrightarrow|b\rangle$ sharply, the equal maximum probability of 2D atom localization decreases, and the resolution reduced.

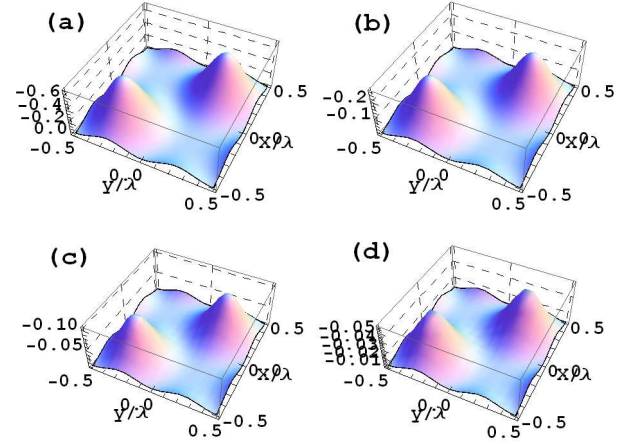


Fig. 3. (Color online) Plots for 2D atom localization: χ'' as a function of (x,y) in dependence on the probe detuning Δ_c . (a) $\Delta_c=-1\gamma$,(b) $\Delta_c=-5\gamma$, (c) $\Delta_c=-10\gamma$, (d) $\Delta_c=-15\gamma$. $\Delta_p=30\gamma$. Other parameters are the same as in Fig.2.

The coupled standing-wave field detuning Δ_c is another considered role in 2D atom localization. In this case, we set $\Delta_p=30\gamma$ and the behavior of the 2D localization is modulated by the coupled standing-wave field detuning Δ_c . In Fig.3, the coupled standing-wave field detuning is turned to $-1\gamma, -5\gamma, -10\gamma$ and -15γ , respectively. And all the other parameters are the same as those in Fig.2. The spikelike pattern occurs in the quadrants I and III of the standing-wave plane from Fig.3(a) to 3(d). Compared to Fig.2, we note that spikelike becomes much more acuity and with the alike decreasing peak maxima pattern from Fig.3(a)

to 3(d). It's worth noting that we obtained the position distribution in the gain process.

As the above observed, we got a clear dependence of the detunings corresponding to the probe and the coupled standing wave fields on the 2D atom localization. Finally, we consider the position distribution dependent the intensities p of SGC, and the corresponding intensities of SGC $p = \cos\theta$ is set as (a) $\theta = \pi/2.1$, (b) $\theta = \pi/2.3$, (c) $\theta = \pi/2.5$, (d) $\theta = \pi/2.7$, as shown in Fig.4 from (a) to (d), respectively. And their corresponding contour plots are shown in Fig.5. Here we set the detunings corresponding to the probe and the coupled standing wave fields are $\Delta_P = 30\lambda$, $\Delta_c = 15\lambda$, and set $\Omega_{p0} = 0.1\gamma$. All the other parameters used here are the same as in Fig.2.

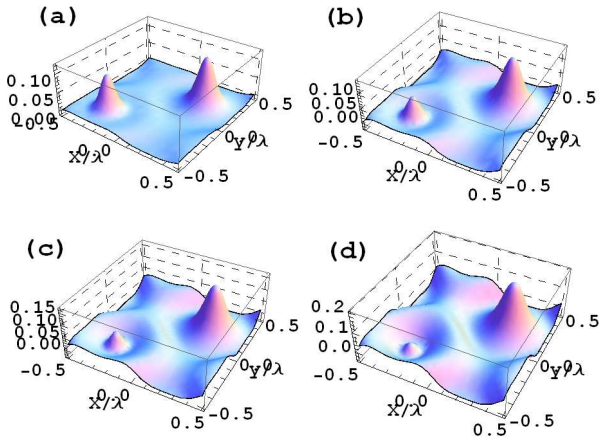


Fig. 4. (Color online) Plots for 2D atom localization: χ'' as a function of (x,y) in dependence on the intensities p of SGC. (a) $\theta = \pi/2.1$, (b) $\theta = \pi/2.3$, (c) $\theta = \pi/2.5$, (d) $\theta = \pi/2.7$. $\delta = 0$, $\eta = \pi/12$, $\Delta_c = 15\lambda$, $\Delta_P = 30\lambda$, $\Omega_{p0} = 0.1\gamma$. All the other parameters are the same as in Fig.2.

It is interesting to compare the results shown in Figs.4 and those shown in Figs.2, in Figs.3. In Fig.4, we obtain two potential positions for the atom localization with one having a higher probability than the other in the absorption process. The peak maxima of the imaginary susceptibility are no longer equal in the four quadrants. As can be seen from Fig.4(a), the peak maxima in quadrant I is higher than the other in quadrant III. When the intensities

of SGC $p = \cos\theta$ with θ be set as $\theta = \pi/2.3$ in Fig.4(b), the high different enhances because of the decrease of the peak maxima in quadrant III. The high different aggravated in Fig.4(c) and Fig.4(d). However, the reason for the aggravation is the same, which the peak maxima is increasing in quadrant I in Fig.4(c) and Fig.4(d).

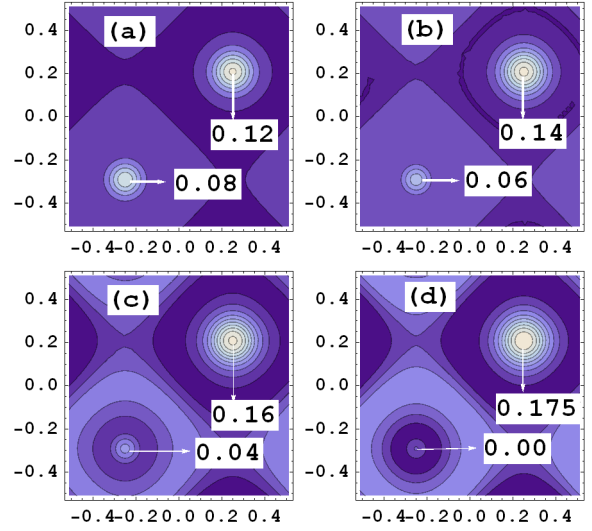


Fig. 5. (Color online) Contour plots for 2D atom localization: χ'' as a function of (x,y) in dependence on the intensities p of SGC. All the parameters in (a) to (d) are the same as in Figs.4, respectively.

In order to get a deeper sight of the role of the intensities p of SGC in 2D atom localization, we show their contour plots in Fig.5. And the corresponding peak maxima values are labeled in Fig.5. From the contour plots shown in Fig.5(a) to Fig.5(d), the values of peak maxima in quadrant I are 0.12, 0.14, 0.16 and 0.175, respectively. And the corresponding values of the peak maxima in quadrant III are 0.08, 0.06, 0.04 and 0. The increasing values in quadrant I and decreasing values in quadrant III demonstrate the effect of the intensities p of SGC on the 2D atom localization. An increasing resolution of 2D atom localization manipulated by the intensities p of SGC is achieved.

In summary, a scheme of 2D atom localization based on the numerical calculations and analyses is obtained. Because of the spatial-dependent atom-field interaction, 2D

atom localization can be realized via measuring the probe absorption. We investigated the conditional position probability distribution of an V-type atom interacting with a weak probe field and two orthogonal standing wave fields. By monitoring position dependent the detunings corresponding to the probe and the standing-wave fields, an equal and tunable peak maxima of position probability distribution is obtained. While a better resolution of position probability distribution is obtained via the intensity p of

SGC. The patterns of spikelike of imaginary susceptibility χ'' in quadrant I and III for 2D atom localization vary differently. And the peak maxima in quadrant I increases gradually while the other one in quadrant III decreases. Compared with the mentioned previous schemes, one peak maxima increasing and other one decreasing for 2D atom localization are the novelty of our scheme.

APPENDIX

The parameters B_i in Eq.(3) are given by the following:

$$\begin{aligned}
B_0 &= P^4(8i + \Delta_c - 3\Delta_p) + \Omega_c^2(5i + \Delta_c - 2\Delta_p)[\Omega_c^2 + (i + \Delta_p)(-2i + \Delta_c - \Delta_p)] + P^2[(i + \Delta_p)(i + \Delta_c)(8i + \Delta_c - 3\Delta_p) + 2\Omega_c^2(5i + \Delta_c - 4\Delta_p)], \\
B_1 &= 2iP^2\{(8i + \Delta_c - 3\Delta_p)[P^2 + (i + \Delta_p)(i + \Delta_c)] + \Omega_c^2(4i + \Delta_c - 3\Delta_p)\}, \\
B_2 &= 2P^4 - [\Omega_c^2 + (i + \Delta_p)(-2i + \Delta_c - \Delta_p)][\Omega_c^2 + (i + \Delta_c)(-3i + \Delta_p)] \\
&\quad + P^2[4 + \Omega_c^2 + \Delta_p(i + \Delta_p) + \Delta_c(5i + \Delta_p)], \\
B_3 &= -iP^4(-4i + \Delta_c - 3\Delta_p) + 2[\Omega_c^2 + (i + \Delta_p)(-2i + \Delta_c - \Delta_p)](1 + \Delta_c^2 + 2\Omega_c^2) - iP^2\{\Delta_p(5 - 3i\Delta_p) \\
&\quad + \Delta_c^2(3i + \Delta_p) + \Omega_c^2(2i - 3\Delta_p) + \Delta_c[9 - \Delta_p(8i + 3\Delta_p) + \Omega_c^2]\}, \\
B_4 &= 8iP^4 + P^2\{-2i[8 + \Delta_c(-4i + \Delta_c) - 4i\Delta_p - 6\Delta_c\Delta_p + \Delta_p^2] + \Omega_c^2(6i + \Delta_c - 5\Delta_p)\} \\
&\quad + [\Omega_c^2 + (i + \Delta_p)(-2i + \Delta_c - \Delta_p)][2(1 - i\Delta_c)(2i + \Delta_c - \Delta_p) + \Omega_c^2(3i + \Delta_c - 2\Delta_p)], \tag{13} \\
B_5 &= P^4(4i + \Delta_c - 3\Delta_p) + [\Omega_c^2 + (i + \Delta_p)(-2i + \Delta_c - \Delta_p)][2(i + \Delta_c)(3 + i\Delta_p) + \Omega_c^2(7i + \Delta_c - 2\Delta_p)] \\
&\quad + P^2\{\Delta_c^2(i + \Delta_p) + \Delta_p(-3 - 5i\Delta_p - 8\Omega_c^2) + 8i(-2 + \Omega_c^2) + \Delta_c[1 + (4i - 3\Delta_p)\Delta_p + 2\Omega_c^2]\}, \\
B_6 &= P^2(6i + \Delta_c - 5\Delta_p) + (5i + \Delta_c - 2\Delta_p)[(-2i + \Delta_c - \Delta_p)(i + \Delta_p) + \Omega_c^2], \\
B_7 &= -4iP^5\Omega_c + iP^3[8 + \Delta_c^2 + \Delta_p(-4i + \Delta_p) - 2\Delta_c(2i + 3\Delta_p)]\Omega_c + p\Omega_c[(2 + i\Delta_c - i\Delta_p + i\Omega_c^2)(i + \Delta_p)] \\
&\quad + [(i + \Delta_c)(2i + \Delta_c - \Delta_p) + \Omega_c^2] + (1 + \Delta_c^2 + 2\Omega_c^2) + \{[4 + (\Delta_c - \Delta_p)^2](i + \Delta_p) + (2i + \Delta_c - \Delta_p)\Omega_c^2\}\Omega_p \\
&\quad + P^2\{(\Delta_c - i)[8 + \Delta_c]^2 + \Delta_p(\Delta_p - 4i) - 2\Delta_c(2i + 3\Delta_p)\} - [12i + 5\Delta_c + (3 + 2i\Delta_p)\Delta_p]\Omega_c^2 - i\Omega_c^4\}\Omega_p \\
&\quad + 2P^4[-2\Delta_c + i(2 + \Omega_c^2)]\Omega_p, \\
B_8 &= -2\Delta_c^3\Delta_p + 6(2 + \Delta_p)^2 - 2\Delta_c\Delta_p(6 + \Delta_p)^2 + \Delta_c^2(6 + 8\Delta_p)^2 + 2[4 - (\Delta_c - 4\Delta_p)(\Delta_c + \Delta_p)]\Omega_c^2 + \Omega_c^4, \\
B_9 &= [4 + (\Delta_c - \Delta_p)^2](1 + \Delta_p)^2 + 2[2 + (\Delta_c - \Delta_p)\Delta_p]\Omega_c^2 + \Omega_c^4, \\
B_{10} &= 12 + \Delta_c^2 - 10\Delta_c\Delta_p + \Delta_p^2 - 4\Omega_c^2.
\end{aligned}$$

China (Grant Nos. 61205205 and 6156508508), the General

* Supported by the National Natural Science Foundation of

Program of Yunnan Provincial Research Foundation of Basic Research for application, China (Grant No. 2016FB009) and the Foundation for Personnel training projects of Yunnan Province, China (Grant No. KKSYS201207068).

† Corresponding author: zhaosc@kmust.edu.cn

- [1] Storey P and Collett M 1993 *Phys. Rev. A*, **47** 405.
- [2] Phillips W D 1998 *Rev. Mod. Phys.*, **70** 721.
- [3] Johnson K S, Thywissen J H, Dekker W H, Berggren K K, Chu A P, Younkin R and Prentiss M 1998 *Science*, **280** 1583.
- [4] Kapale K T, Qamar S and Zubairy M S 2003 *Phys. Rev. A*, **67** 023805.
- [5] Herkommer A M, Carmichael H J and Schleich W P 1996 *Quantum Semiclass. Opt.*, **8** 189.
- [6] Qamar S, Zhu S Y and Zubairy M S 2000 *Phys. Rev. A*, **61** 063806.
- [7] Qamar S, Zhu S Y and Zubairy M S 2000 *Opt. Commun.*, **176** 409.
- [8] Paspalakis E and Knight P L 2001 *Phys. Rev. A*, **63** 065802.
- [9] Sahrai M, Tajalli H, Kapale K T and Zubairy M S 2005 *Phys. Rev. A*, **72** 013820.
- [10] Liu C P, Gong S Q, Cheng D C, Fan X J and Xu Z Z 2006 *Phys. Rev. A*, **73** 025801.
- [11] Agarwal G S and Kapale K T 2006 *J. Phys. B*, **39** 3437.
- [12] Cheng D C, Niu Y P, Li R X and Gong S Q 2006 *J. Opt. Soc. Am. B*, **23** 2180.
- [13] Xu J and Hu X M 2007 *Phys. Lett. A*, **366** 276-281.
- [14] Xu J and Hu X M 2007 *Phys. Rev. A*, **76** 013830.
- [15] Kunze S, Dieckmann K and Rempe G 1997 *Phys. Rev. Lett.*, **78** 2038.
- [16] Quadt R, Collett M and Walls D F 1995 *Phys. Rev. Lett.*, **74** 351.
- [17] Qamar S, Mehmood A and Qamar S 2009 *Phys. Rev. A*, **79** 033848.
- [18] Marte M A M and Zoller P 1992 *Appl. Phys. B*, **54** 477.
- [19] Carmichael H J *An Open Systems Approach to Quantum Optics: Lecture Notes in Physics* (Springer-Verlag, Berlin, 1993).
- [20] Paspalakis E, Terzis A F and Knight P L 2005 *J. Mod. Opt.*, **52** 1685.
- [21] Evers J, Qamar S and Zubairy M S 2007 *Phys. Rev. A*, **75** 053809.
- [22] Qamar S, Evers J and Zubairy M S 2009 *Phys. Rev. A*, **79** 043814.
- [23] Kapale K T and Zubairy M S 2006 *Phys. Rev. A*, **73** 023813.
- [24] Wan R G, Kou J, Jiang L, Jiang Y and Gao J Y 2011 *J. Opt. Soc. Am. B*, **28** 10.
- [25] Dutta B K, Panchadhyayee P and Mahapatra P K 2013 *Laser Phys.*, **23** 045201.
- [26] Ivanov V and Rozhdestvensky Y 2010 *Phys. Rev. A*, **81** 033809.
- [27] Wan R G, Kou J, Jiang L, Jiang Y and Gao J Y 2011 *Opt. Commun.*, **284** 985.
- [28] Ding C, Li J, Yang X, Zhang D and Xiong H 2011 *Phys. Rev. A*, **84** 043840.
- [29] Rahmatullah and Qamar S 2013 *Phys. Rev. A*, **88** 013846.
- [30] Ding C, Li J, Zhan Z and Yang X 2011 *Phys. Rev. A*, **83** 063834.
- [31] Li J, Yu R, Liu M, Ding C and Yang X 2011 *Phys. Lett. A*, **375** 3978-3985.
- [32] Ding C, Li J, Yu R, Hao X and Wu Y 2012 *Optics Express*, **20** 7870-7885
- [33] Wu J C, Liu Z D, Zheng J and WANG H Q 2013 *Chin. Phys. Lett.*, **30** 034205.
- [34] Wu J C, Liu Z D and Zheng J 2013 *Chin. Phys. B*, **22** 044203.
- [35] Javanainen J 1992 *Europhys. Lett.*, **17** 407.
- [36] Agarwal G S *Quantum Optics, Springer Tracts in Modern Physics*, **70** (Springer, Berlin, 1974) p.95.
- [37] Harris S E 1989 *Phys. Rev. Lett.*, **62** 1033; Zibrov A S, Lukin M D, Nokonov D E 1995 *Phys. Rev. Lett.*, **75** 1499.
- [38] Zhu S Y and Scully M O 1996 *Phys. Rev. Lett.*, **76** 388.
- [39] Paspalakis E, Kylstra N J and Knight P L 1999 *Phys. Rev. Lett.*, **82** 2079; 2000 *Phys. Rev. A*, **61** 045802.
- [40] Wu J H, Gao J Y and Xu J H 2005 *Phys. Rev. Lett.*, **95** 057401; Zibrov A S, Lukin M D, Hollberg L 1996 *Phys. Rev. Lett.*, **76** 3935.
- [41] Hong T, Cramer C, Nagourney W and Fortson E N 2005 *Phys. Rev. Lett.*, **94** 050801; Zhou P and Swain S 1998 *J. Opt. Soc. Am. B*, **12** 2593.
- [42] Jia K N, Liu Z B, Liang Y, Tong D M and Fan Xi J 2012 *Acta Phys. Sin.*, **61** 064204.

- [43] Joshi A and Xiao M 2005 *Eur. Phys. J. D*, **35** 547.
- [44] Zhao S C 2011 *JETP Letters*, **94** 347.
- [45] Bennett C H and Divincenzo D P 2000 *Nature (London)*, **404** 247; Paternostro M, Kim M S and Knight P L 2005 *Phys. Rev. A*, **71**022311.
- [46] Kocharovskaya O, Matsko A B and Rostovtsev Y 2001 *Phys. Rev. A*, **65** 013803.
- [47] Yablonovitch E 1989 *Phys. Rev. Lett.*, **58**2059.
- [48] Meystre P and Sargent III M, *Elements of Quantum Optics (3rd ed)*, (Springer-Verlag, Berlin, 1999).
- [49] Lee H, Polynkin P, Scully M O and Zhu S Y 1997 *Phys. Rev. A*, **55** 4454
- [50] Menon S and Agarwal G S 1999 *Phys. Rev. A*, **61** 013807.